Supplementary Information for:

An Ultraflexible Energy Harvesting-Storage System for Wearable Applications

Sakeena Saifi,[1,2] Xiao Xiao,[1,2] Simin Cheng,[1,2] Haotian Guo,[1,2] Jinsheng Zhang,[3] Peter Müller-Buschbaum,[3] Guangmin Zhou,[1,2] Xiaomin Xu,[1,2]* Hui-Ming Cheng[4,5,6]*

[1]Institute of Materials Research, Shenzhen International Graduate School, Tsinghua University, Shenzhen 518055, China

[2]Shenzhen Geim Graphene Center, Tsinghua-Berkeley Shenzhen Institute, Tsinghua University, Shenzhen 518055, China

[3]Technical University of Munich, TUM School of Natural Sciences, Department of Physics, Chair for Functional Materials, James-Franck-Str. 1, 85748 Garching, Germany

[4]Shenzhen Key Laboratory of Energy Materials for Carbon Neutrality, Shenzhen Institute of Advanced Technology, Chinese Academy of Sciences, Shenzhen 518055, China

[5]Faculty of Materials Science and Energy Engineering, Shenzhen Institute of Advanced Technology, Shenzhen 518055, China

[6]Shenyang National Laboratory for Materials Science, Institute of Metal Research, Chinese Academy of Sciences, Shenyang 110016, China

*Correspondence should be sent to: cheng@imr.ac.cn

and xu.xiaomin@sz.tsinghua.edu.cn

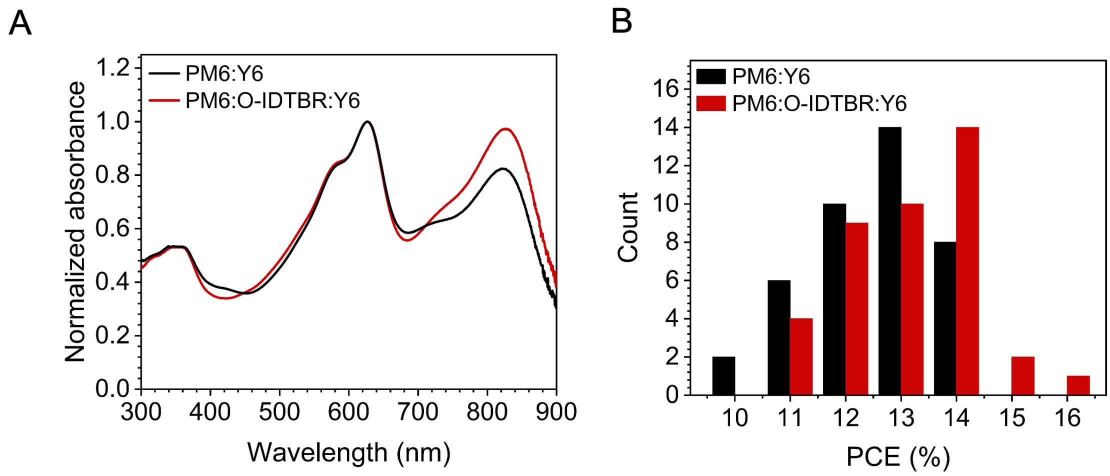

Figure S1. Binary and ternary blend OPV devices. (A) Absorption spectra of PM6:Y6 binary blend (black) and PM6:O-IDTBR:Y6 ternary blend (red). (B) Statistical results of the PCE obtained from ultraflexible OPVs based on binary (black) and ternary (red) blends (40 samples for each).

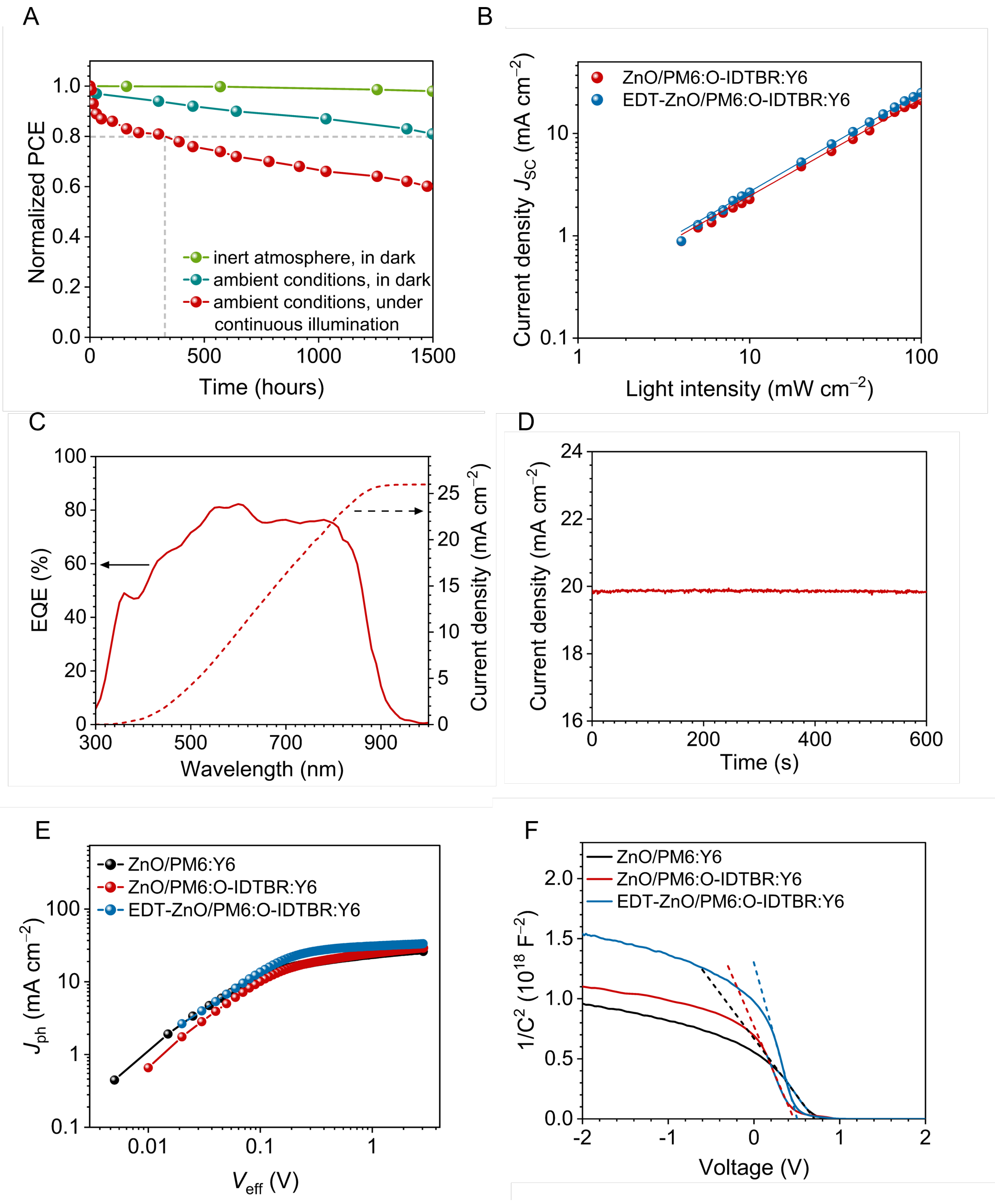

Figure S2. Performance of the ultraflexible OPVs. (A) Stability of OPVs based on PM6:Y6 binary blend under the inert atmosphere in the dark (green), in ambient conditions in the dark (blue), and in ambient conditions under a continuous illumination of 50 mW cm^{-2} (red). (B) Light intensity dependance of J_{SC}. A comparative analysis between devices using pure ZnO (red) and EDT-ZnO (blue) as the electron transport layer. (C) Integrated J_{SC} (dashed line) from EQE spectrum of PM6:O-IDTBR:Y6 ternary blend (solid line). (D) Stability of J_{SC} with respect to time. (E) J_{ph}-V_{eff} curves of devices based on ZnO/PM6:Y6 (black), ZnO/PM6:O-IDTBR:Y6 (red), and EDT-ZnO/PM6:O-IDTBR:Y6 (blue). (F) Mott-Shockley plot of OPV devices based on ZnO/PM6:Y6 (black), ZnO/PM6:O-IDTBR:Y6 (red) and EDT-ZnO/PM6:O-IDTBR:Y6 (blue) (dashed lines represent the linear fitting).

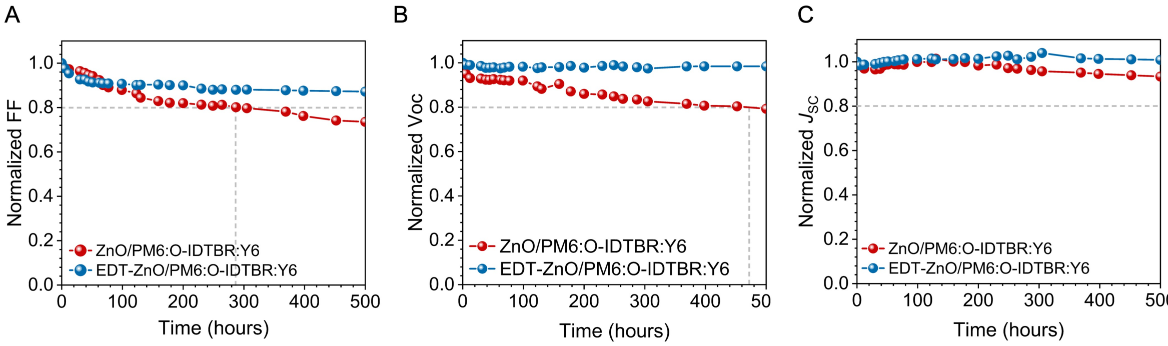

Figure S3. Photostability of OPV devices. Photostability of ultraflexible OPV devices having ZnO (red) and EDT-ZnO (blue) as respective electron transport layers. The devices were based on PM6:O-IDTBR:Y6 ternary blend. Normalized (A) fill factor, (B) V_{OC}, and (C) J_{SC}, respectively.

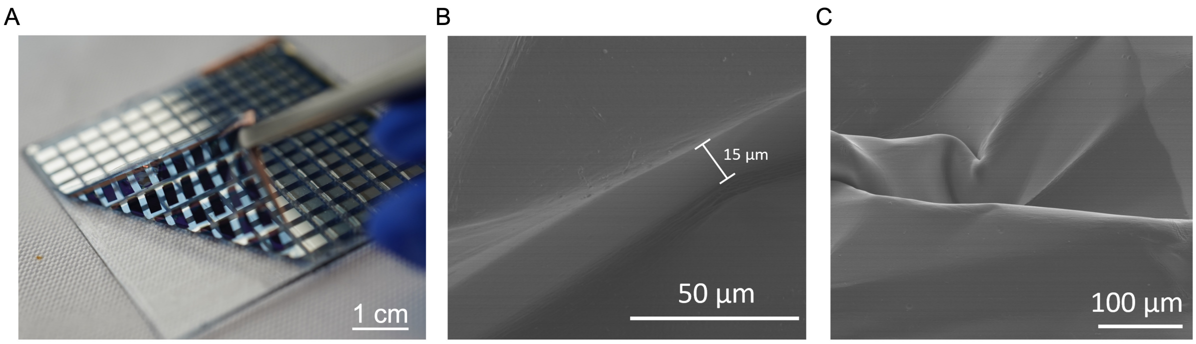

Figure S4. Ultraflexible OPV module. (A) Photograph of a 5x5 cm^2 OPV module being delaminated from the supporting glass slide. (B-C) Scanning electron microscopic (SEM) images of an ultraflexible OPV before (B) and after (C) the mechanical durability test of 1000 bending cycles at 1 mm bending radius.

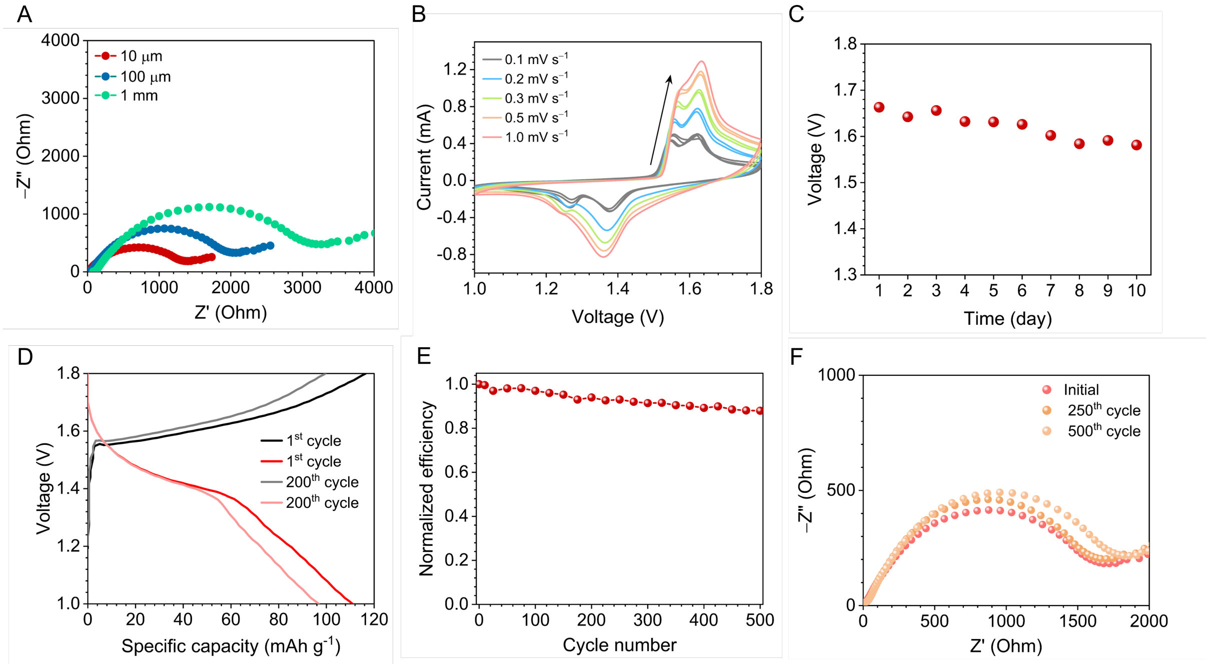

Figure S5. Performance of ultrathin ZIB. (A) Nyquist plots of ZIBs featuring hydrogel electrolyte of different thicknesses: 10 µm (red), 100 µm (blue), and 1 mm (cyan). (B) Cyclic voltammogram of an 85 µm-thick ZIB at variable scan rates. (C) Storage stability of the 85 µm-thick flexible ZIB under ambient conditions. (D) Charge-discharge curves of a flexible ZIB at both the 1st and 200th cycles. (E) Coulombic efficiency of the 85 µm-thick ZIB recorded over continuous bending cycles at a bending radius of 1 mm. The results highlight mechanical durability of the thin ZIB. (F) Nyquist plots of the 85 µm-thick ZIB after subjected to 250 and 500 bending cycles (orange), contrasting with its initial unstrained state (red).

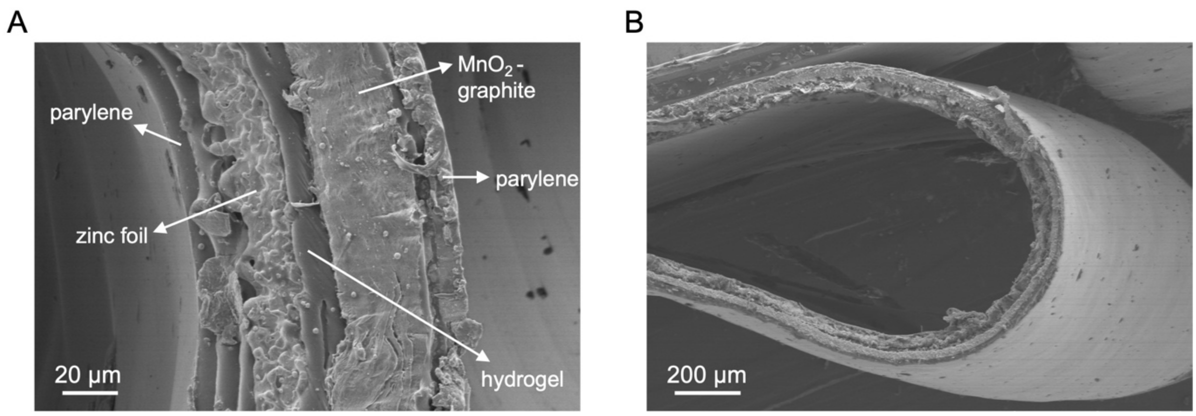

Figure S6. SEM images of a sub-100 µm thick ZIB. (A) Cross-sectional SEM image of the as-prepared ZIB, highlighting each layer component. (B) Cross-sectional SEM image of the ZIB under bending strain, demonstrating mechanical compliance and structural integrity.

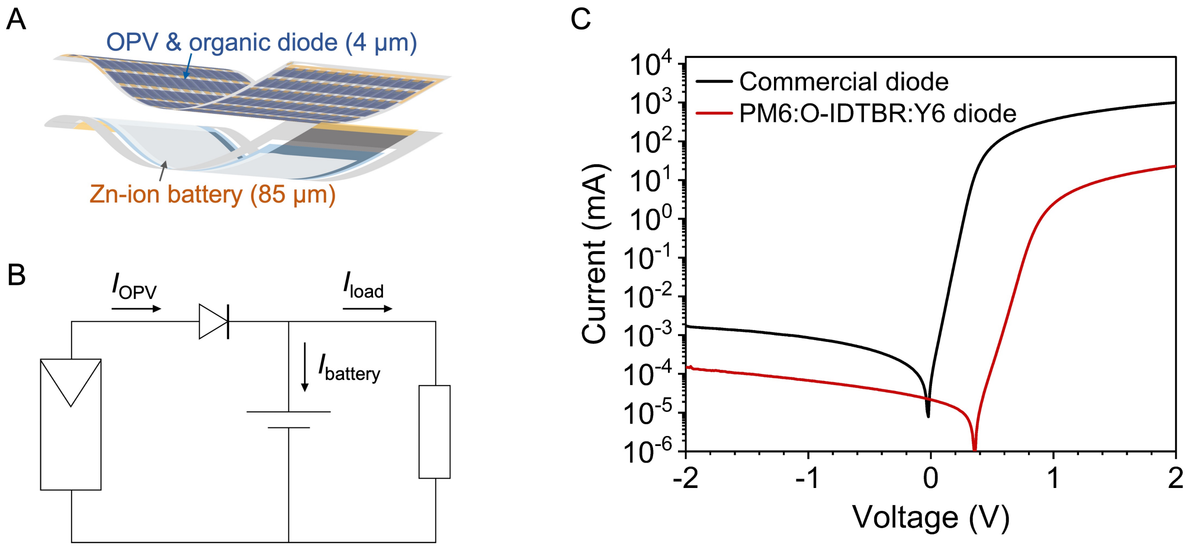

Figure S7. FEHSS with integrated organic diode. (A) Schematic showing the layout of the OPV module, the current control diode, and the flexible Zn-ion battery. (B) Circuit diagram of the integrated system. (C) *J-V* characteristic of the current control diode (red) and a commercial Si diode (black), measured under room lighting.

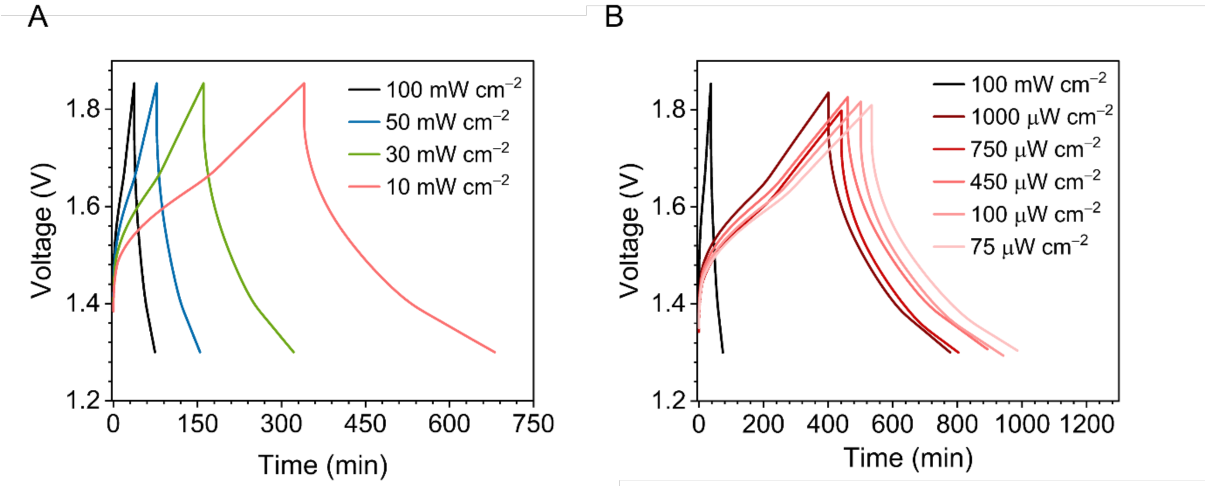

Figure S8. Charge-discharge profiles of FEHSS. (A) Under different light intensities. (B) Under low light intensities approximating indoor light conditions (red traces), in comparison with the profile obtained under 1 sun illumination condition, i.e., 100 mW cm^{-2} (black). The FEHSS consists of a 6.72 cm^2 ultraflexible OPV module, and a ZIB battery.

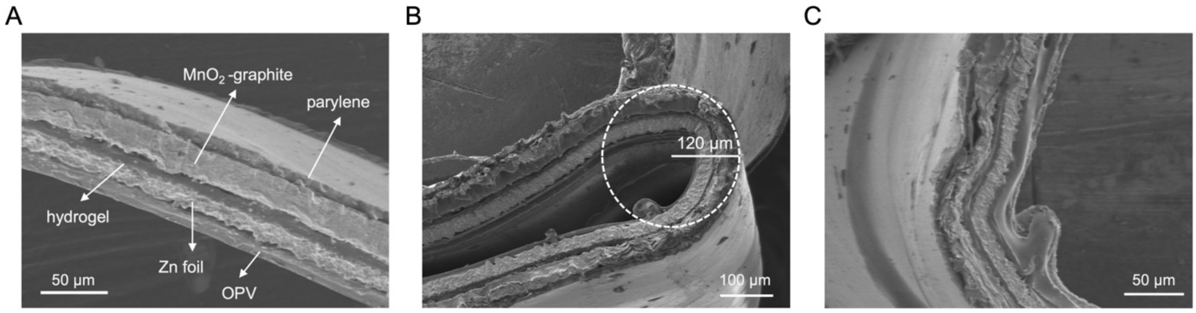

Figure S9. SEM images of integrated FEHSS. (A) Cross-section SEM image of an as-prepared FEHSS, highlighting each layer component. (B) Cross-sectional SEM image of the FEHSS under bending strain, demonstrating a bending radius down to 120 μm. (C) Cross-sectional SEM image of the FEHSS after 500 cycles of repeated bending test.

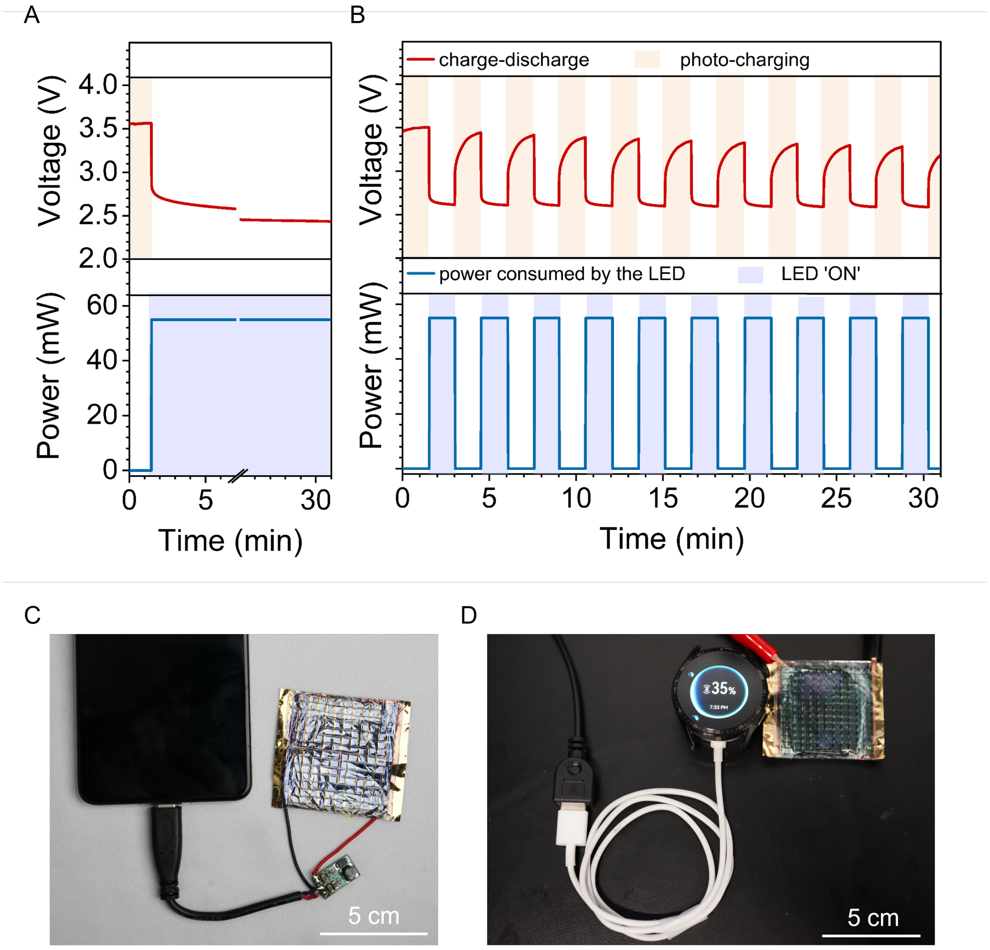

Figure S10. (A) Voltage-time curve (top), and power-time curve (bottom) of the FEHSS powering an LED for over 30 minutes without photo-charging. The top plot shows the voltage drop of FEHSS as it continuously discharges power to the LED without light illumination. The bottom plot shows the power consumed by the LED over 30 minutes. (B) Voltage-time curve (top), and power-time curve (bottom) of the FEHSS connected to an LED. The top plot shows the charge-discharge curve of the FEHSS as the LED is turned on and off at 1.5-min intervals to allow the FEHSS to charge in between cycles. The bottom plot shows the power consumed by the LED when it is turned on. The results show that with 1.5-min intervals under low light intensity, i.e., 10 mW cm^{-2} and powering the LED, the FEHSS's voltage output dropped to 2.65 V after 30 min, while it took only 7 min to drop to the same value without photo-charging. (C-D) Photographs showing the system layout for charging a smartphone (C), and a smartwatch (D) by FEHSS. In (C), the printed regulation board consists of a DC-DC converter to stabilize the voltage output at 5.0 V. In (D), a wireless charger (HUAWEI WATCH charging cradle CP81-1) was used, connected to the FEHSS with an USB cable.

Table S1. Performance parameters of ultraflexible OPV single units.

	V_{OC} (V)	J_{SC} (mA cm^{-2})	FF (%)	PCE (%)	PCE_{max} (%)	α	n	N_A ($\times10^{16}$ cm^{-3})
Binary-blend, ZnO ETL	0.79 ± 0.02	23.4 ± 0.2	72.6 ± 0.5	13.5 ± 0.2	13.70	0.95	1.30	3.1
Ternary-blend, ZnO ETL	0.81 ± 0.01	25.0 ± 0.2	73.6 ± 0.3	14.9 ± 0.3	15.20	0.99	1.22	1.78
Ternary-blend, EDT-ZnO ETL	0.81 ± 0.01	26.2 ± 0.1	75.2 ± 0.3	15.7 ± 0.2	16.18	1.005	1.08	1.14

Note: The active area of all devices is 0.04 cm^2. Data were averaged from 10 devices for each.

Table S2. Summary on the performance of reported flexible OPVs and flexible OPV modules.

	Thickness (μm)	Active area (cm^2)	P_{areal}* ($mW\ cm^{-2}$)	Active materials	Substrate	Ref.
Flexible OPVs	175	1	7.17	PTB7-Th:p-DTS(FBTTH2)2:$PC_{71}BM$	PET	1
	175	2	5.66	PTB7:PC_{71} BM	PET	2
	175	10	5.83	PTB7-Th:p-DTS(FBTTH2)2:$PC_{71}BM$	PET	3
	125	1	17.07	PM6:L8-BO	PET	4
	125	1	16.71	PBDB-TF: BTP-eC9	PEN	5
	125	1	16.54	PM6:BTP-4Cl-12	PET	6
	125	1	15.82	PM6:BTP-eC9:$PC_{71}BM$	PET	7
	125	1	14.29	PM6:Y6	PET	8
	125	1	13.61	PM6:Y6	PET	9
	125	1	12.26	PBDB-TF:IT-4F	PET	10
	125	1	12.16	PTB7-Th: COi8DFIC:$PC_{71}BM$	PET	11
	125	1	3.52	PBDTTTz-4:$PC_{71}BM$	PET	12
	125	1	2.25	PTB7-TH : $PC_{61}BM$	PET	13
	125	1	2.7	P3HT:$PC_{71}BM$	PET	14
	125	1	1.93	BDTTT-C-T: $PC_{71}BM$	PET	15
	125	1.04	9.77	PBDB-T:ITIC	PET	16

	125	1.2	5.85	P3HT:ICBA	PET	17
	125	4	7.09	PTB7:$PC_{71}BM$	PET	18
	125	4	1.93	P3HT:$PC_{71}BM$	PEN	19
Ultra-flexible OPVs	2.5	1.94	6.97	PTzNTz:$PC_{71}BM$	PI/Ag	20
	3	1	8.8	PBDTTT-OFT:$PC_{71}BM$	Parylene	21
	3	1.2	5.85	PTzNTZ-BOBO:$PC_{71}BM$	Parylene	22
	3	1.36	11.46	PBDBT:ITIC	PI	23
	3	2.97	8.43	PBDTTT-OFT: IEICO-4F	Parylene	24
	4	3.2	8.08	PM6:IT-4F	Parylene	25
	4	1.28	13.8	PM6:O-IDTBR:Y6	Parylene	This work
		6.72	10.3	PM6:O-IDTBR:Y6	Parylene	
		16	4.9	PM6:O-IDTBR:Y6	Parylene	

*Note: To ensure a direct comparison, all P_{areal}^* values were calculated using the effective working area of the devices.

Table S3. Overall efficiency of FEHSS consisting of one ZIB, when charged under different light intensities.

OPV module	Light intensity (mW cm^{-2})	Charging time (hours)	Capacity (mAh)	Energy density (mWh cm^{-2})	Overall efficiency (%)
6.72 cm^2	100	0.6	3.0	2.65	1.15
	65	0.95	3.5	3.00	1.25
	50	1.2	3.7	3.14	1.35
	30	2.0	3.8	3.25	1.41
	10	5.6	4.0	3.42	1.59
1.28 cm^2	100	1.0	5.27	4.5	5.27
	65	1.5	5.5	4.7	6.61
	50	2.0	5.7	4.89	6.68
	30	3.3	5.8	4.97	6.86
	10	10	5.9	5.05	6.91

Table S4. Summary of the performance of reported FEHSSs based on solar energy harvesters and battery storage systems.

FEHSS type	1/Thickness (mm^{-1})	PCE (%)	Energy density ($mWh\ cm^{-2}$)	Specific capacity ($mAh\ cm^{-2}$)	Diode	Overall efficiency (%)	Ref.
PSC-ZIB	6.66	11.1	0.0016	-	No	5.28	26
PSC-ZIB	2.85	18.27	5.11	3.63	No	-	27
SiPV-LIB	0.77	15.8	2.7	0.5	No	7.61	28
SiPV-LIB	0.4	6	6.98	1.84	No	-	29
FIED	3.85	3.5	-	-	Yes	-	30
OPV-LIB	4.0	5.49	1.25	3.5	No	-	31
OPV-ZIB	11.1	16.18	5.82	3.88	Yes	6.91	This work

Note: PSC stands for perovskite solar cell, ZIB stands for zinc-ion battery, SiPV stands for silicon photovoltaic, LIB stands for lithium-ion battery, FIED stands for fiber-shaped integrated energy device, and OPV stands for organic photovoltaic.

Supplementary References

1 Zhao, Y. *et al.* A sequential slot-die coated ternary system enables efficient flexible organic solar cells. *Solar RRL* **3**, 1800333 (2019).

2 Huang, Y. C., Cha, H. C., Chen, C. Y. & Tsao, C. S. A universal roll-to-roll slot-die coating approach towards high-efficiency organic photovoltaics. *Prog. Photvolt.: Res. Appl.* **25**, 928-935 (2017).

3 Zhang, J. *et al.* Enhancing performance of large-area organic solar cells with thick film via ternary strategy. *Small* **13**, 1700388 (2017).

4 Wang, Z. *et al.* Manipulating the macroscopic and microscopic morphology of large-area gravure-printed ZnO films for high-performance flexible organic solar cells. *Energy Environ. Mater.* **7** (2024).

5 Liu, X. *et al.* Fluidic manipulating of printable zinc oxide for flexible organic solar cells. *Adv. Mater* **34**, 2106453 (2022).

6 Han, Y. *et al.* 12.42% Monolithic 25.42 cm^2 flexible organic solar cells enabled by an amorphous ITO-modified metal grid electrode. *Adv. Mater* **34**, 2110276 (2022).

7 Zeng, G. *et al.* Realizing 17.5% efficiency flexible organic solar cells via atomic-level chemical welding of silver nanowire electrodes. *J. Am. Chem. Soc.* **144**, 8658-8668 (2022).

8 Pan, W. *et al.* An efficiency of 14.29% and 13.08% for 1 cm^2 and 4 cm^2 flexible organic solar cells enabled by sol–gel ZnO and ZnO nanoparticle bilayer electron transporting layers. *J. Mater. Chem. A* **9**, 16889-16897 (2021).

9 Wang, Z. *et al.* High power conversion efficiency of 13.61% for 1 cm^2 flexible polymer solar cells based on patternable and mass-producible gravure-printed silver nanowire electrodes. *Adv. Funct. Mater* **31**, 2007276 (2021).

10 Han, Y. *et al.* Efficiency above 12% for 1 cm^2 flexible organic solar cells with Ag/Cu grid transparent conducting electrode. *Adv. Sci* **6**, 1901490 (2019).

11 Wang, G. *et al.* Synergistic optimization enables large-area flexible organic solar cells to maintain over 98% PCE of the small-area rigid devices. *Adv. Mater* **32**, 2005153 (2020).

12 Helgesen, M. *et al.* Making ends meet: flow synthesis as the answer to reproducible high-performance conjugated polymers on the scale that roll-to-roll processing demands. *Adv. Energy Mater* **5**, 1401996 (2015).

13 Liu, K. *et al.* Roll-coating fabrication of flexible organic solar cells: comparison of fullerene and fullerene-free systems. *J. Mater. Chem. A* **4**, 1044-1051 (2016).

14 Krebs, F. C., Gevorgyan, S. A. & Alstrup, J. A roll-to-roll process to flexible polymer solar cells: model studies, manufacture and operational stability studies. *J. Mater. Chem* **19**, 5442 (2009).

15 Cheng, P. *et al.* Comparison of additive amount used in spin-coated and roll-coated organic solar cells. *J. Mater. Chem. A* **2**, 19542-19549 (2014).

16 Meng, X. *et al.* A general approach for lab-to-manufacturing translation on flexible organic solar cells. *Adv. Mater* **31**, 1903649 (2019).

17 Mao, L. *et al.* Flexible large-area organic tandem solar cells with high defect tolerance and device yield. *J. Mater. Chem. A* **5**, 3186-3192 (2017).

18 Zuo, L., Zhang, S., Li, H. & Chen, H. Toward highly efficient large-area ITO-free organic solar cells with a conductance-gradient transparent electrode. *Adv. Mater* **27**, 6983-6989 (2015).

19 Galagan, Y. *et al.* ITO-free flexible organic solar cells with printed current collecting grids. *Sol. Energy Mater. Sol. Cells* **95**, 1339-1343 (2011).

20 Jiang, Z. *et al.* Durable ultraflexible organic photovoltaics with novel metal-oxide-free cathode. *Adv. Funct. Mater* **29**, 1808378 (2019).
21 Xu, X. *et al.* Thermally stable, highly efficient, ultraflexible organic photovoltaics. *Proc. Natl. Acad. Sci.* **115**, 4589-4594 (2018).
22 Jinno, H. *et al.* Self-powered ultraflexible photonic skin for continuous bio-signal detection via air-operation-stable polymer light-emitting diodes. *Nat. Commun* **12** (2021).
23 Jiang, Z. *et al.* Highly efficient organic photovoltaics with enhanced stability through the formation of doping-induced stable interfaces. *Proc. Natl. Acad. Sci.* **117**, 6391-6397 (2020).
24 Takakuwa, M. *et al.* Direct gold bonding for flexible integrated electronics. *Sci. Adv* **7**, eabl6228 (2021).
25 Sun, L. *et al.* All-solution-processed ultraflexible wearable sensor enabled with universal trilayer structure for organic optoelectronic devices. *Sci. Adv* **10**, eadk9460 (2024)
26 Jinxin Bi, J. Z. *et al.* A highly integrated flexible photo-rechargeable system based on stable ultrahigh-rate quasi-solid-state zinc-ion micro-batteries and perovskite solar cells. *Energy Storage Mater.* **51**, 239-248 (2022).
27 Zhao, J. *et al.* A safe flexible self-powered wristband system by integrating defective MnO_2 nanosheet-based zinc-ion batteries with perovskite solar cells. *ACS Nano* **15**, 10597-10608 (2021).
28 Um, H.-D. *et al.* Monolithically integrated, photo-rechargeable portable power sources based on miniaturized Si solar cells and printed solid-state lithium-ion batteries. *Energy Environ. Sci.* **10**, 931-940 (2017).
29 Ostfeld, A. E., Gaikwad, A. M., Khan, Y. & Arias, A. C. High-performance flexible energy storage and harvesting system for wearable electronics. *Sci. Rep.* **6**, 26122 (2016).
30 Sun, H. *et al.* Integrating photovoltaic conversion and lithium ion storage into a flexible fiber. *J. Mater. Chem. A* **4**, 7601-7605 (2016).
31 Lee, Y.-H. *et al.* Wearable textile battery rechargeable by solar energy. *Nano Lett.* **13**, 5753-5761 (2013).